Iranian Journal of Hydrogen & Fuel Cell 2(2019) 171-184

Iranian Journal of Hydrogen & Fuel Cell

IJHFC

Journal homepage://ijhfc.irost.ir

Synthesis of a Zr-Co-Y based chemical getter and evaluation its vacuum preserving, sorption characteristics, and hydrogen absorption

Mehrdad Fattahzade, Ali Kaflou*, Valiollah Dashtizad

Department of Advanced Materials and Renewable Energies, Iranian Research Organization for Science and Technology, Tehran, Iran

Article Information

Article History:

Received:
7 Jan 2020
Received in revised form:
14 Mar 2020
Accepted:
6 Apr 2020

Keywords

Chemical Getter
Zirconium-Cobalt Powder
Sievert apparatus
Hydrogen Storage
Vacuuml

Abstract

In this research, a Zr-Co based chemical non-evaporable getter (NEG) was synthesized via mechanical alloying. A mixture with a 75 %Wt. Zr, 22 %Wt. Co, and 3 %Wt. Y composition (Zr75Co22Y3) was selected, mixed, and milled up to 42 h. The obtained powder was pressed in a tablet form. The sample was placed in a well-sealed vacuum chamber that was evacuated to 1.5×10^{-5} mmHg. Then, the sample was subjected to different heat treatments (at various temperatures and times) for activation. Results revealed that the final vacuum for the Y36030 sample (Zr75Co22Y3 activated at 360ºC for 30 min) and the Y28030 sample (Zr75Co22Y3 activated at 280 ºC for 30 min) were 5.95×10^{-6} and 9.9×10^{-6} mmHg, respectively. After finishing the heat treatment, vacuum variation versus time was recorded in the range of 0.001-0.2 mmHg, the time for Y36030, Y28030, and a no-getter was 3088, 510, and 345 seconds, respectively. Sievert results showed that Y36030 absorbed 1.5 %Wt H_2 at 45 bar while Y28030 absorbed 1.05 %Wt. H_2. After removing the pressure, the remaining amount of hydrogen for Y36030 and Y28030 was 0.7 and 0.55 %Wt., respectively.

1. Introduction

Using getters is one of the most convenient means to achieve a high vacuum and preserve it for a long time. A chemical getter is a suitable candidate for many purposes such as use in MEMS[1] , solar receivers, Cern laboratory accelerators, UHV[2] , XHV[3] systems, etc. [1-4].

*Corresponding Author's Fax: +982144144307
E-mail address: ali.kaflou@irost.ir

doi: 10.22104/ijhfc.2020.1614.1199

[1]Micro Electro-Mechanical Systems
[2]Ultra-High Vacuum
[3]Extreme High Vacuum

Appropriate material selection from chemical and economic aspects are mandatory parameters. In many cases the necessity to remove a great number of active gases as well as confronting the surface limitation in a vacuum chamber leads to the use of bulk getters (non-evaporable getters or NEG) instead of evaporable ones. Often this type of getters (NEG) is in tablet form, which is produced by the powder metallurgy technique [2].

Zirconium based getters are widely used due to their high capacity and ability to absorb a wide range of active gases such as H_2, H_2O, O_2, CO, CO_2, Hydrocarbons, etc. [2-4]. One of the most common elements used for alloying with Zr is Co, Co improves the thermodynamics and kinetics properties of Zr based getters [1, 5, 6]. Zhang et al. reported that the amorphous state of Zr-Co based alloy is due to the relatively large size of its interstitial sites, which results in more sorption capacity compared to the crystalline state [7]. Alloying zirconium with cobalt results in the formation of a Zr_3Co phase, which is considered an appropriate candidate for sorption and storage of hydrogen isotopes [8, 9]. Zavaliy et al. showed that the Zr_3Co compound can absorb hydrogen until the formation of saturated hydrides, more than either zirconium or cobalt in their elemental forms [10].

The effect of rare earth elements on sorption characteristics of getters has been studied by many researchers [1,11,12]. In almost in all cases, adding a trace amount of rare earth elements significantly improved the getter performance. The effect of adding such elements has been studied by several researchers [1, 6]. Although these elements are added in low amounts, they rigorously enhance the getter performance.

One of the latest studies in this field involved adding a trace amount of Ce/La (1.5 %Wt. of each element) to a Zr-Co based getter. Adding Ce/La improved the sorption characteristics of the getter significantly (the starting temperature of the activation decreased about 60ºC) [6].

In addition to the selection of an appropriate composition, secondary treatments, such as refining particles to achieving high surface area, are very beneficial. The specific surface area of the getters correlates with their Kinetics and sorption capacity. One of the most useful and rapid ways to accelerate the activation of getter material is to reduce the grain size, which accordingly increases the grain boundary and reduces the penetration path. This can be achieved by milling base materials or their mixes in a high-energy ball mill. Decreasing grain size will also increase the specific surface area, and consequently, increase the absorption capacity [6]. Valdre et al. claimed that a Zr-based getter produced by milling in a high energy apparatus showed increased sorption speed [13]. Milling can produce intermetallic compounds, nanostructures, and amorphous phases, all of which play important roles in improving sorption characteristics. Neelima et al. assessed the influence of mechanical milling on the physical properties of Zr2Co11 [14]. They found increasing milling time decreased particle size from 200 μm to 120 μm, and partial amorphization was detected at 6 hours. Producing porous getters is also one of the most popular methods of enlarging the surface area, which can increase the kinetic of absorption [15, 16].

Because of the very high chemical activity of getter materials and the fact that their contamination during synthesis is unavoidable, a barrier layer (mostly oxide/carbide compounds) forms on their surfaces [2, 3]. Samples are subjected to a certain heat treatment (known as the activation process) to eliminate this layer and initiate the absorption [1-3]. Activation conditions play an important role in getter performance of absorbing active gases [6, 17-19].

Hydrogen, having a very small atomic structure, is the most important cause of leakage in vacuum systems. Thus, hydrogen sorption by getters is very important. Barta et al. reported that adding 0.5 %Wt. yttrium to zirconium produced higher nucleation of hydride compounds, which resulted in a refinement of the microstructure [20].

Since adding trace amounts of rare earth elements has a great effect on improving Zr-Co based getters and there is a resemblance in chemical properties

between yttrium and rare earth elements as well as the fact that there is has been no study regarding the synthesis of ZrCoY getter, Zr75Co22Y3 was chosen for investigation. The aim of this work is to study the effect of adding yttrium to Zr-Co base getter alloy on vacuum preserving and hydrogen sorption. The powders of zirconium, cobalt, and yttrium were mixed, milled and activated in different conditions and their vacuum preserving time and sorption characteristics were studied.

2. Experimental procedure

The Zr and Co powders were obtained from Sigma Aldrich, and the Y powder was commercial grade. Table 1 shows the complete specification of the powders.

Table1 Specification of the powders.

Element	Zr	Co	Y
Purity	99.9%	99.9%	98%
Particle size	<150 µm	<200 µm	≤200 µm

The Zr75Co22Y3 compound (75 %wt. Zr, 22 %wt. Co, and 3 %wt. Y) was mixed in a Turbula mixer for 20 min, then transferred to a hardened vial (~60 Rc) in argon atmosphere. Ar was purged up to 4 bars 3 times to minimize environmental contamination. Milling was done at different intervals up to 42 h. All preparation stages of the samples (weighing, mixing, and charging in the vial) were done in a glove box under atmosphere control (Ar 99.999%). The effect of milling conditions on getter performances was discussed in our previous work [17].

After milling, the powder was pressed into a tablet form with a 10 mm diameter at 1.5 GPa pressure. The weight of the samples was fixed at 1.3 gr. In the next step, samples were placed in a well-sealed reactor connected to a high vacuum bench and then heated by a fine heating control system (±1ºC). The evacuation was continued until reaching a pressure of 1.5×10^{-5} mmHg. After stabilizing the pressure, the getter was subjected to a certain heat treatment cycle. The heating procedure consisted of two stages: first, heating at 100ºC for 30 min, to remove trapped gases (bake-out stage), and subsequently, heating at temperatures shown in Table 2 (activation stage). During activation, the pressure variation versus time was recorded. The samples are coded as shown in Table 2. The first three digits show temperature and the next two show the time of the heat treatment. Samples containing yttrium are marked with the letter Y at the beginning of the code.

After finishing the activation procedure, the vacuum bench was disconnected from the pumps, and the vacuum preserving time between 0.001 and 0.2 mmHg was recorded. Finally, samples were taken off under an argon atmosphere. The morphology of the samples was determined by a Mira II-TESCAN FESEM equipped with an Energy Dispersive Spectrometer (EDS). The microstructure of the samples was studied by TEM (Philips-CM200 FE). The adsorption capacity of the getters was measured using a Bellsorb Mini II instrument, and finally, the hydrogen storage of the samples was investigated using a Sievert type apparatus at 298 K.

3.Results and discussion

3.1 Activation results

Fig. 1 A and B show the pressure variation versus

Table 2 The characteristics of activated samples.

Sample Code	Activation time(min)	Activation Temperature (°C)	Sample information
Y28030	30	280	42 h milled, with adding 3 %Wt. yttrium
Y28080	80	280	
Y32080	80	320	
Y36030	30	360	
Y36080	80	360	

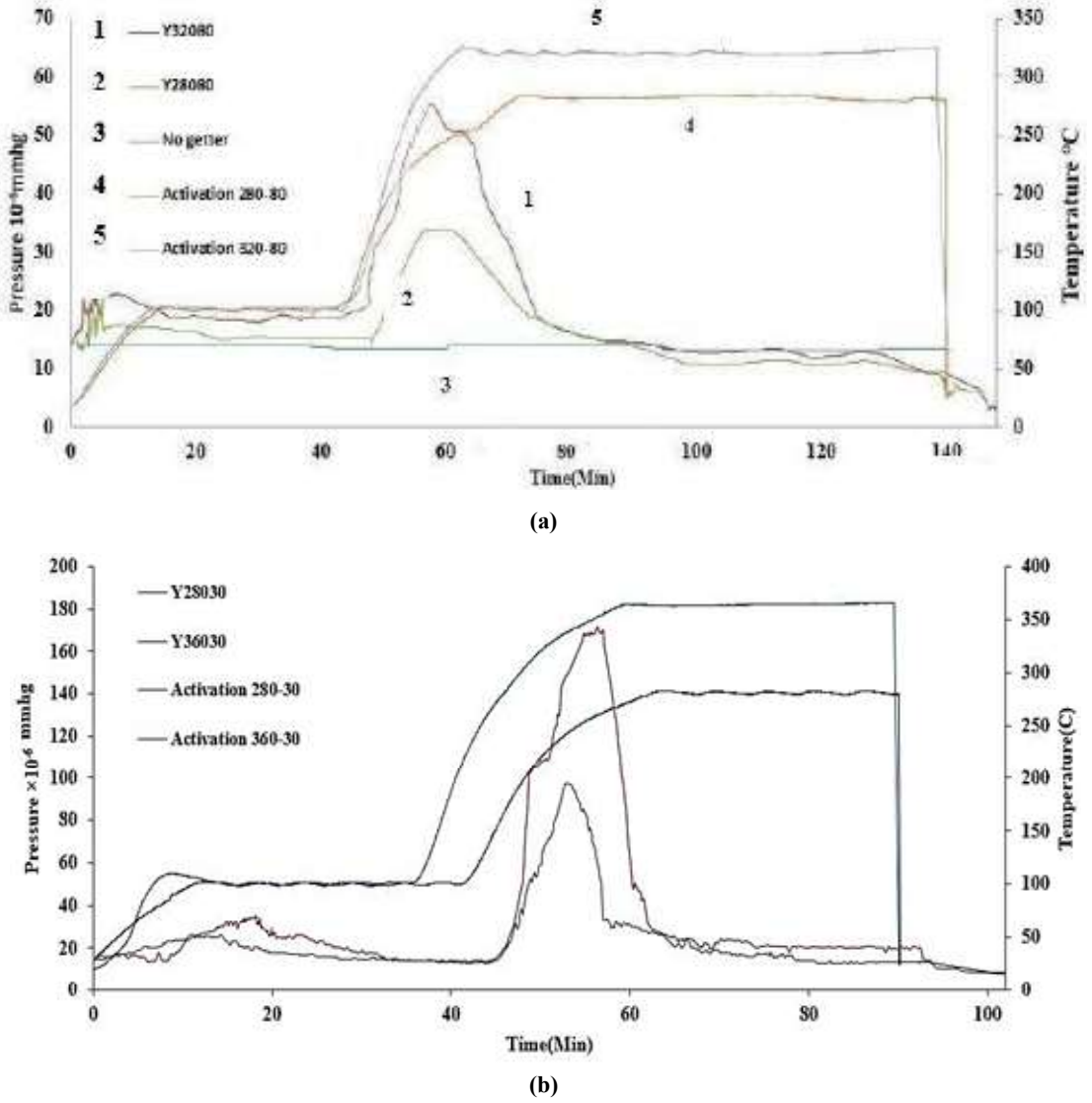

Fig. 1 Pressure variation at a) temperatures of 280 and 320ºC for 80 min and b) temperatures of 280 and 360 ºC for 30 min.

time and temperature for samples through the heating process. The P-t-T curve (Pressure-Time-Temperature) showed two peaks during heating: the first appeared around 100 ºC (due to the release of trapped gasses) [6], and the second started at temperatures about 250 ºC. Since the activation conditions were kept the same for all samples, the area under the P-t curve is somehow related to the volume of released gases. Thus, by having a greater surface area, the sorption capacity of the getters will be increased [18]. The pressure variation in the no-getter case remained almost without any change, which emphasizes the effect of getters on pressure fluctuations. The area under the curve was calculated and is shown in Table 3.

According to Table 3, the highest area under the curve belonged to Y36030. Increasing the activation time in the samples activated at 280 ºC for 30 and 80 min increased the area by 22%, and the final vacuum decreased by 37%. By increasing the activation temperature from 280 to 360 ºC at 30 min, the area increased by 51%, and the final vacuum decreased by 39%. Thus, it can be concluded that the activation temperature plays a more important role than the activation time on the sorption characteristics, similar to the results stated by Matolin et al. [19]. According

Table 3 Data extracted from Fig. 1.

Sample code	The area under the curve mmHg.min	Final vacuum mmHg	Vacuum preserving time (s)
Y32080	2831.92	5.98×10^{-6}	2784
Y36030	3277.41	5.95×10^{-6}	3088
Y28030	2180.552	9.9×10^{-6}	510
Y28080	2668.74	6.2×10^{-6}	1059

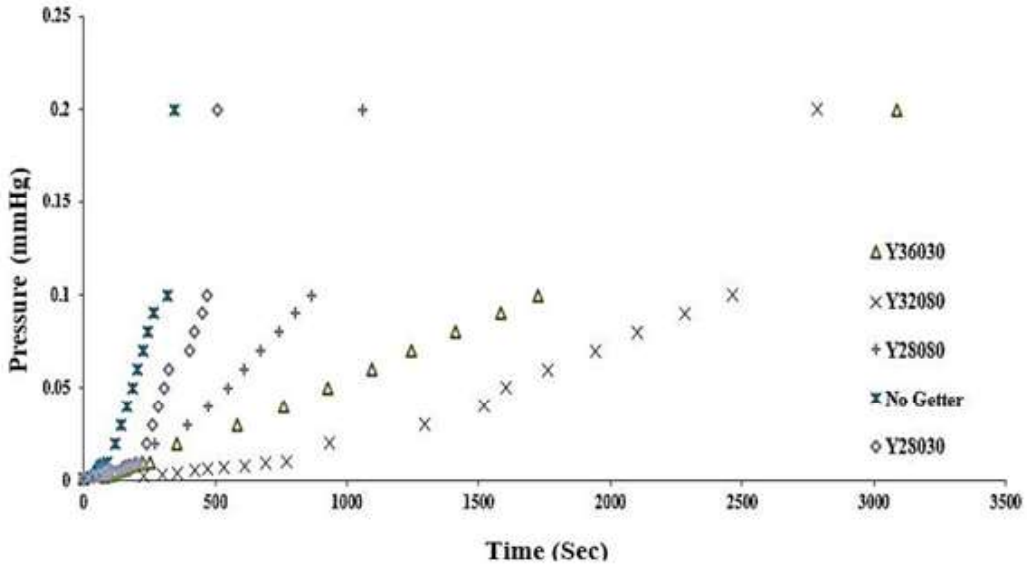

Fig 2. Vacuum preserving time for different samples.

to these results, there is a direct relationship between the increased area and lowering the final vacuum for Zr-Co based getters.

The vacuum preserving time from 0.001 to 0.2 mmHg for the different samples is shown in Fig. 2 and Table 3. At 3088 seconds, Y36030 has the most vacuum preserving time, the time for Y28080 and Y28030 were 2784 and 1059 seconds, respectively. This result shows the effect of activation temperature on the vacuum preserving time. Based on Fig. 2, increasing the time and temperature of the activation increases the vacuum preserving time. In the case of the no-getter, the vacuum preserving time for the system with a total volume of 7 lit was 345 seconds, while it was 3088 seconds for Y36030, an eight fold increment.

3.2. Microstructure evaluation

Microstructures of Y28030 and Y36030 are shown in Fig. 3. In Y28030, the particle sizes are between 3 and 5 microns, while for Y36030, some nanometric particles have formed on the surface of the larger particles. These nano-particles can be formed by nucleation and growth in the amorphous phase [17]. Fig. 4 and Table 4 show the elemental analysis at point A. As can be seen, the chemical composition at this point is very close to the Zr_3Co phase. The Zr_3Co has an orthorhombic structure, which results in it having more interstitial sites and more sorption capacity [21-23]. Forming the Zr_3Co via XRD analysis was assessed and previously proven by the same team [6, 21]. Fig. 5 shows the result of the TEM micrograph for Y36030 and Y28030. The SAED pattern for Y28030 shows it has remained almost amorphous and does not show any crystalline rings or spots. Y36030 exhibits the presence of crystalline rings and spots, which confirms its polycrystallinity (crystalline nature) [21]. Y36030 and Y28030 were studied via line and map scans to monitor the presence of oxygen and distribution of other elements, outcomes are shown in Figs. 6 and

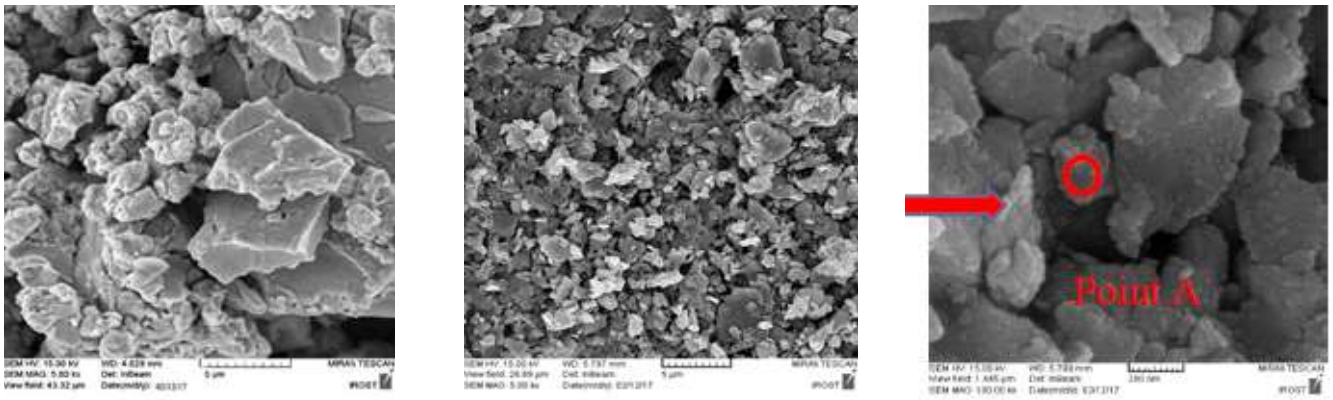

(a) **(b)** **(c)**

Fig. 3. The microstructure of a) Y28030 at 5 Kx magnification, b) Y36030 at 5 Kx magnification, and c) Y36030 at 100 Kx magnification.

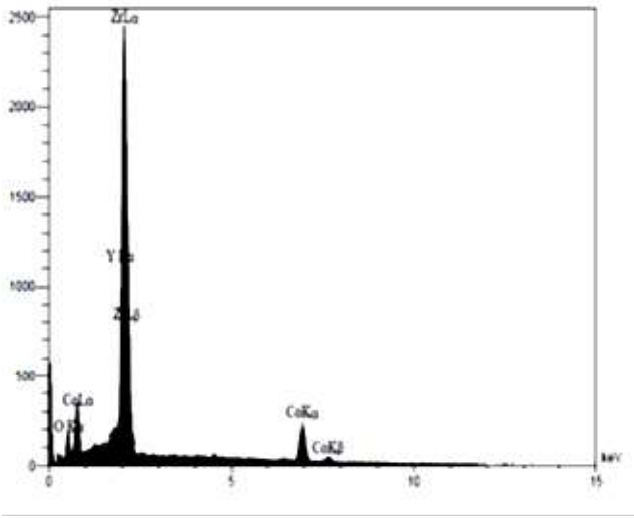

Fig. 4 Results of elemental analysis at point A.

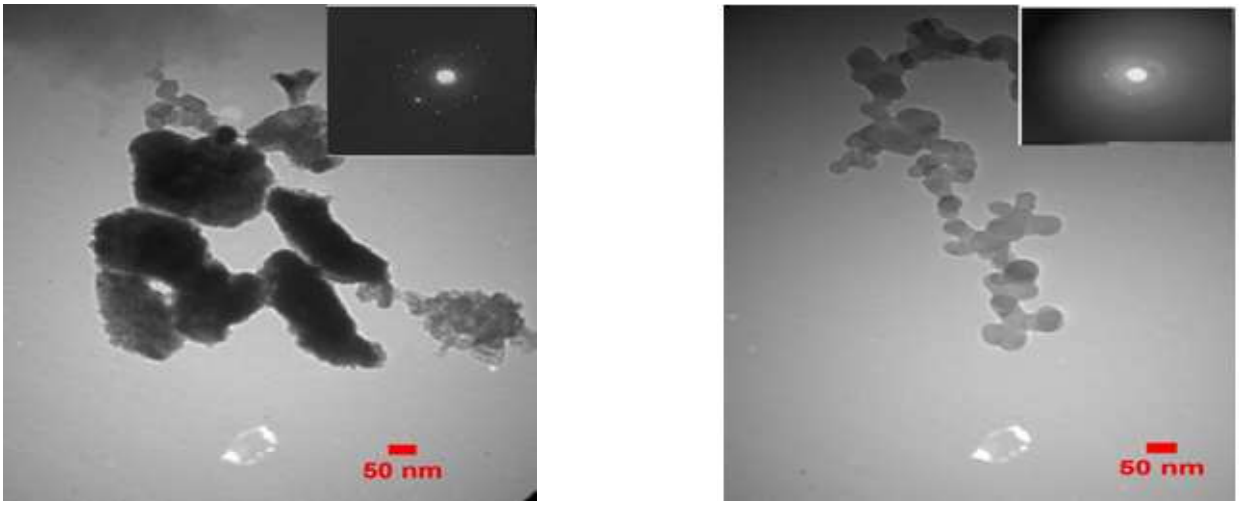

(a) **(b)**

Fig. 5 TEM results of a) Y28030 and b) Y36030.

Table 4 Results of elemental analysis at point A.

Elements	%Wt
O wt%	21.18
Zr wt%	53.25
Co wt%	17.58
Y wt%	3.59

7. According to these figures, less oxygen is presents at the surface of Y36030 compared to Y28030, which can result in better sorption performance of the getter. According to Fig. 6, the amount of cobalt on the scanned area (near the surface) had fluctuations and increased up to 40% at some points, which is similar to the findings of Petti et al. for a Zr-Co base getter [22]. In both samples, the yttrium amount remained virtually constant at near to 3 %Wt.

Fig. 8 shows the surface of Y36030 before and after activation at 500x magnification. There are some cracks on the surface of the sample after activation (Fig. 8 B) in comparison with the sample before activation (Fig. 8 A), as pointed out in the figure. One reasons for the formation of these cracks can be the formation of Zr_3Co [21, 23], other important reasons are hydrogen sorption and hydride forming [24-26]. This result shows the suitability of Y36030 for hydrogen absorption.

The results of hydrogen sorption for Y36030 and Y28030 are shown in Fig. 9. Both samples reached a saturation level up to 45 bar and both have a hysteresis loop. A hysteresis loop usually forms in metals (metallic elements) because of strains related

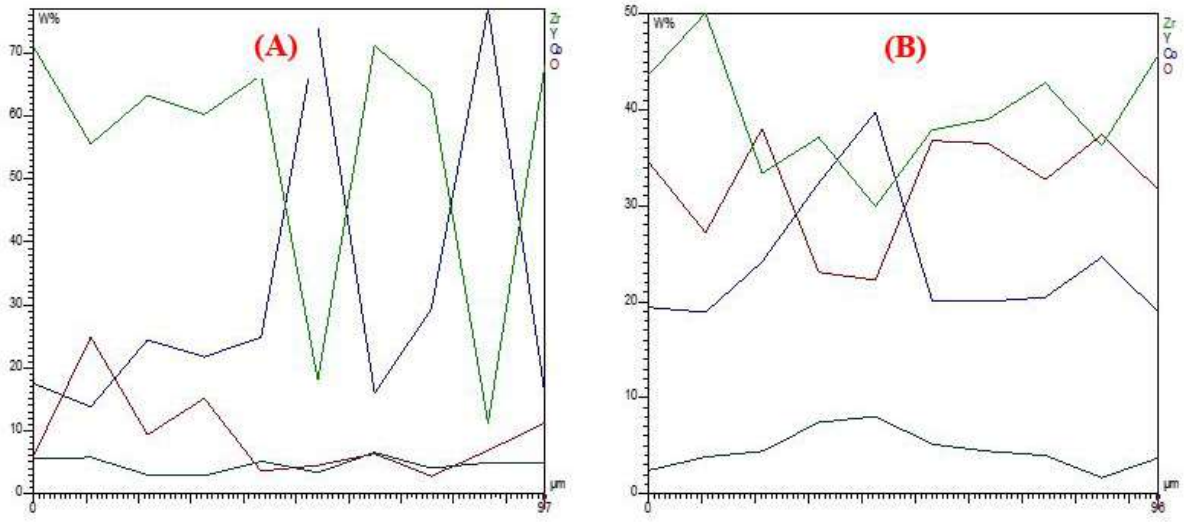

Fig. 6 Line scan analysis of a) Y36030 and b) Y28030.

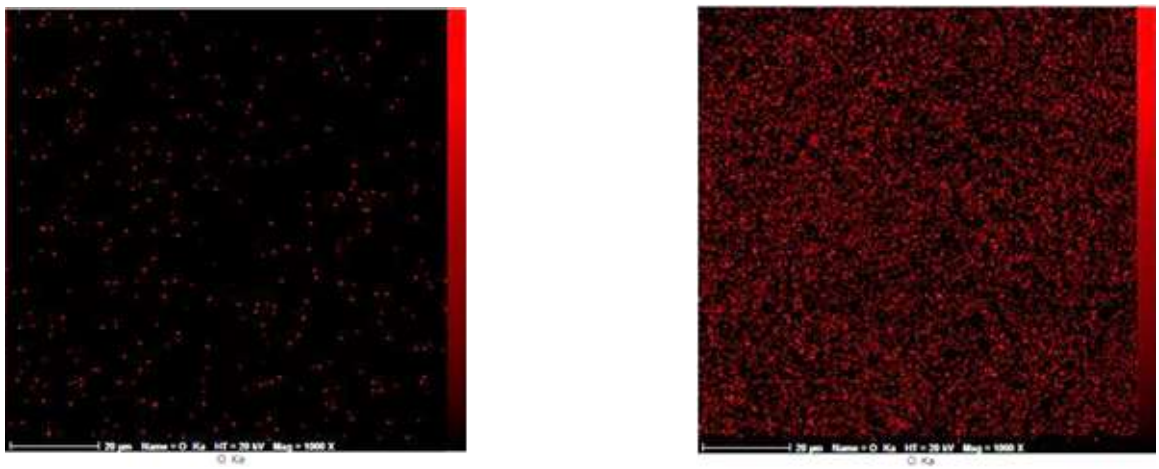

(a) **(b)**

Fig. 7 Map scan analysis of a) Y36030 and b) Y28030.

to hydrogen sorption, hydride forming, and hydrides decomposition [27]. Since hysteresis loops have formed, some hydrogen atoms have remained in the getters during the sorption/desorption process (reversible sorption needs heating at high temperature and vacuum for desorption). The difference between the sorbed and desorbed hydrogen atoms causes the hysteresis loop [28-30]. Y36030 reached its saturation level at 45 bar, while this pressure was 43 bar for Y28030. The amount of sorbed hydrogen for Y36030 and Y28030 were 1.5 and 1.05 %Wt., respectively. Moreover, the remaining hydrogen in Y36030 and Y28030, after removing the pressure of hydrogen, was 0.71 and 0.55, respectively. Thus, based on these results, Y36030 performed better for hydrogen sorption and storage.

The results of nitrogen sorption (BET test) on Y36030 and Y28030 at a pressure near to the

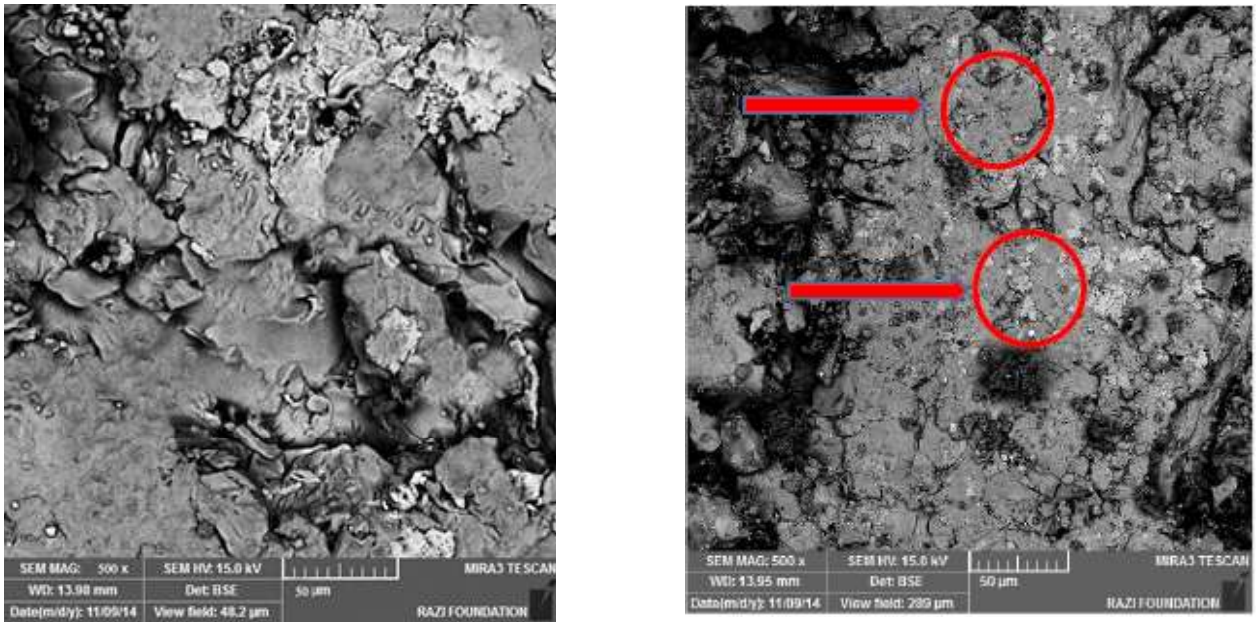

(a) (b)

Fig. 8 The surface of Y36030 a) before activation and b) after activation.

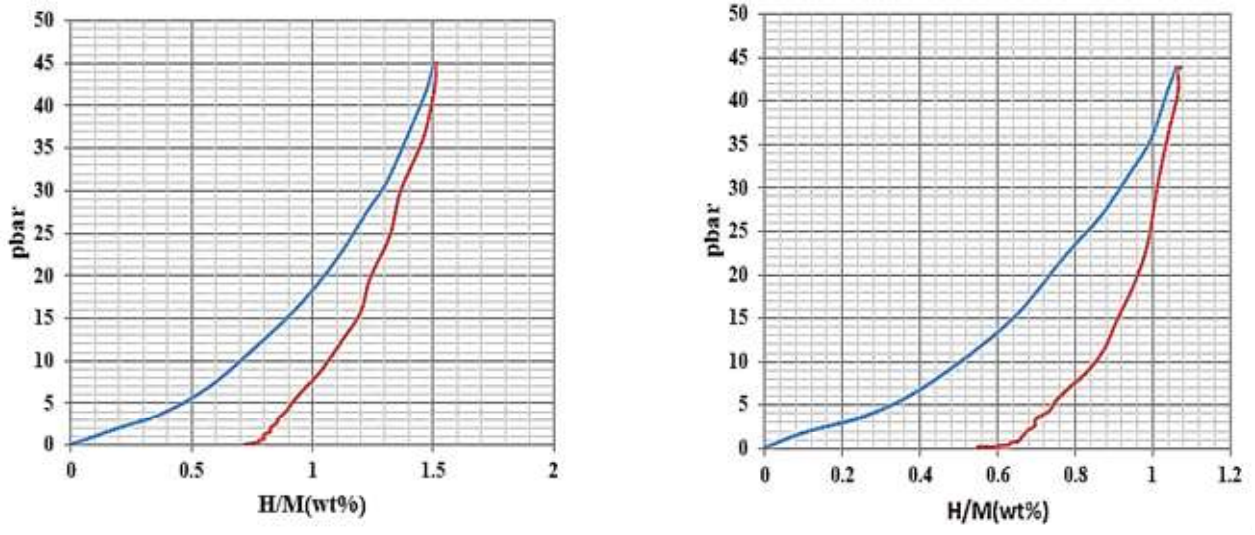

(a) (b)

Fig. 9 Sorption/Desorption of A) Y28030 and B) Y36030.

equilibrium pressure are shown in Fig. 10. Usually, the adsorption/desorption diagrams consist of four stages. The first stage is usually upright and is known as the Henry's law region, the next stage is linear where P/P0 varies from 0.05 to 0.3. The intersection between the first and second stages is known as the monolayer adsorption region. The next stage relates to the hysteresis loop formation, at this level the pores between 1 to 100 nm are filled with liquid nitrogen. After reaching the hysteresis loop at a parallel state with the horizontal axis, large pores are filled, and finally, with a sharp increase, the diagram ends [31]. Y36030 and the Y28030 had sharp increases at P/P0 of 0.85. This was based on the continuous progression from multilayer adsorption to capillary condensation in which the smaller pores became filled with liquid nitrogen. This phenomenon occurred when the saturation vapor pressure in a small pore was reduced by the effect of surface tension according to the Kelvin equation [32].

At a P/P0 higher than 0.90, the adsorption capacity barely increased and no large diameter pores existed. The saturated adsorption capacity for Y36030 and Y28030 were 14 and 10 cm3, respectively. Porosities were classifies into three groups based on their sizes, where micropores are less than 2 nm, mesopores are between 2 and 50 nm, and macropores are larger than 50 nm. This classification is published by IUPAC [16]. The adsorption isotherms for both samples correspond to type IV in the IUPAC classification, which represents the mesoporous structural characteristic [16, 21].

Specific surface area is calculated from equation (1):

$$S_B=(V_m N_a a)/(m \times 22400) \quad (1)$$

Where Vm is the volume of adsorbed nitrogen from the surface, Na is the Avogadro constant, a is the surface area of the adsorbed gas's atom (0.162 nm^2 for nitrogen), and m is the mass of the tested sample, 22400 represents the occupied volume (ml) by one moll of the gas at standard conditions [32].

Fig. 11 shows the BET results of Y36030 and Y28030. The value of the $p/Va(P_0-P)$ for Y36030 at P/P_0 = 0.22 and for Y28030 at P/P_0 = 0.2 deviated from the linear form and increased nonlinearly, the reason for this phenomenon was an increase in pressure, which subsequently enhanced the volume of adsorbed gas [30].

Nitrogen adsorption for both samples can be explained by multilayer adsorption, which is presented in the BET model. In this model, there is equilibrium between the adsorption and desorption. Thus, the total amount of adsorbed gas consists of the adsorbed quantity of each layer.

SB is calculated from the BET equation and based on this equation, the surface area is related linearly to the volume of adsorbed gas by one layer (V_m). The slope of this diagram is related inversely with

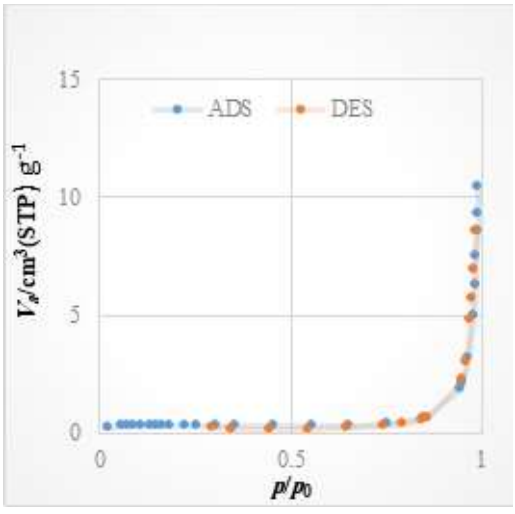

(a)

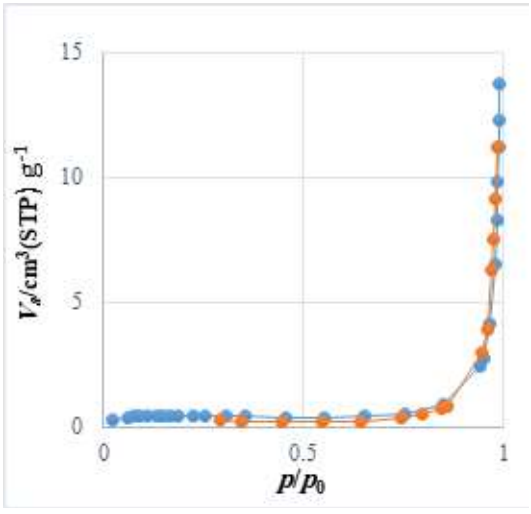

(b)

Fig.10 Adsorption/ Desorption of a) Y28030 and b) Y36030.

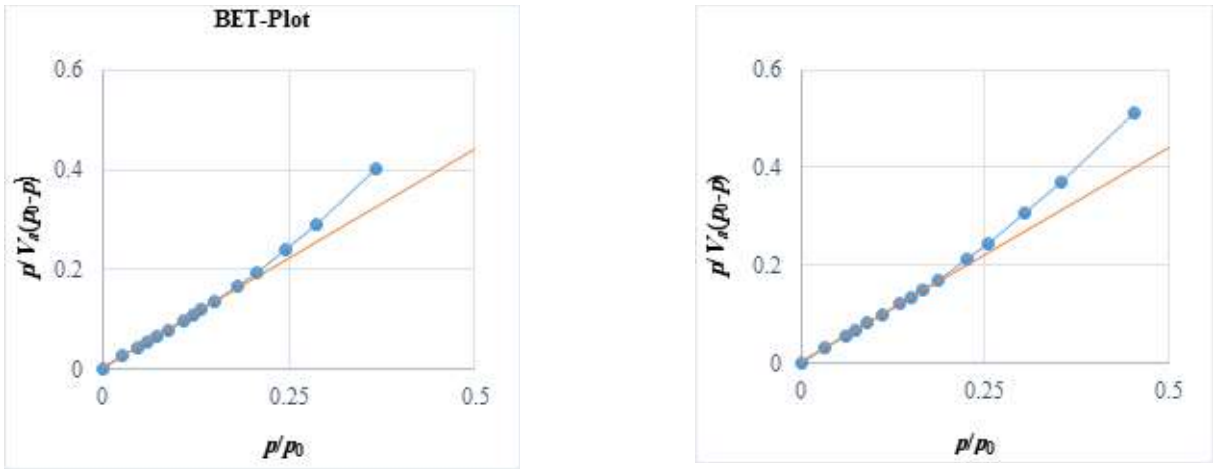

(a) (b)

Fig. 11 BET results of a) Y36030 and b) Y28030.

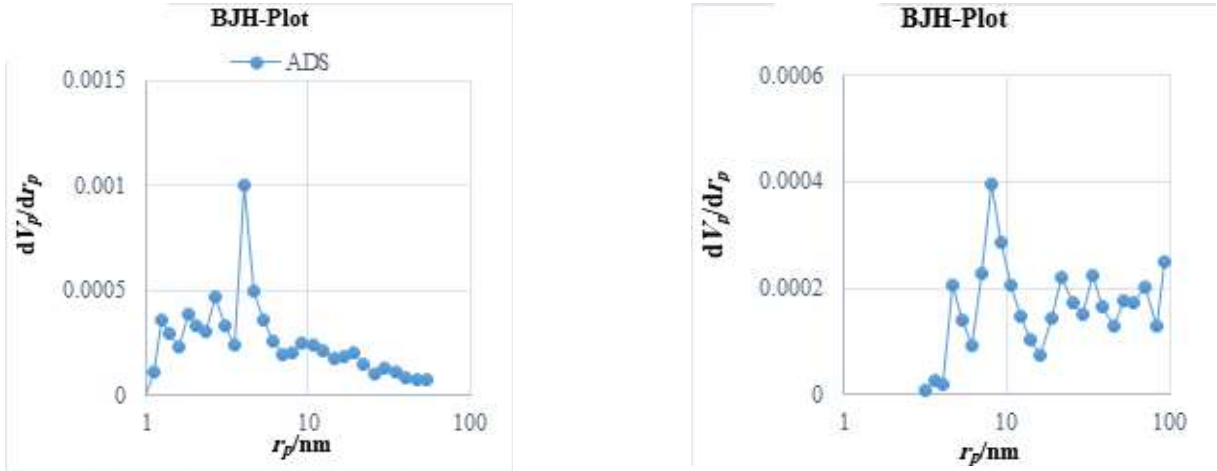

(a) (b)

Fig. 12 BJH results of a) Y36030 and b) Y28030.

the V_m. As the slope is greater, the V_m and surface area would be smaller. Therefore, since the slope of Y36030 was lower than Y28030, its surface area is greater as is shown in Table 5.

Fig.12 shows the pore size distribution (PSD) of Y36030 and Y28030. The range of the pore sizes for Y36030 was between 1 and 53 nm and between 2 and 100 nm for Y28030. Therefore, it can be concluded that according to the higher activation temperature of Y36030, having smaller pores can be related to the nucleation and growth in the amorphous phase [21]. According to Table 5, the mean diameter of the porosities are less than 10 nm while the primary powders were micron size. The reason for this observation may be related to the nucleation and growth of nano-particles, this result (formation of nano-crystallites) is also confirmed by the FESEM results (Fig. 3 c), TEM results (Fig. 5), and the form of the BET graph (Fig. 10), which correlates with type IV (mesoporous). This difference can be explained by the growth of nano-crystallites and the porosity between them. A similar observation is presented by Heidary et al. [21].

According to Table 5 and BET results based on the volume of sorbed nitrogen, the comparison between the volumes of the samples is as follows: Y36030> Y32080 > Y28080 > Y28030.

The extracted data from Figs. 11 and 12 are gathered in Table 5. According to this table, the average pore size for Y36030 is lower than Y28030, which can be

be caused by the nucleation and growth of nanoparticles. The specific surface area and the volume of the absorbed gas (V_m) of Y36030 are greater than that of Y28030, which results in more sorption capacity.

Table 5 Specific surface area and average pore diameter for Y36030 and Y28030.

Sample code	SB(m^2/gr)	rp(nm)	V_m(cm^3/gr)
Y36030	75.23	4.76	0.5361
Y28030	61.27	7.92	0.4336
Y28080	65.43	8.32	0.44after that 74
Y32080	69.52	6.53	0.4614

The favorable effect of Y can be explained by thermodynamic data. The Gibbs free energy of formation of Y_2O_3 and ZrO_2 at standard conditions (1 bar, 298.15 K) are -1816.65 kJ/mol [33] and -1039.7 kJ/mol [34], respectively. Regarding this significant difference, one can conclude that the formation of Y_2O_3 is more feasible than ZrO_2 in the same conditions after the dissociation of the oxide layer. As mentioned before, the getter requires an activation process. This process is accomplished by heating the getter in a well-sealed reactor connected to a vacuum bench. During activation, the oxide and carbide compounds shall be dissociated and diffuse into the bulk to gain the active surface for adsorption. In the presence of Y, the temperature required for this purpose is reduced. In other words, yttrium can facilitate this step by forming Y_2O_3 (the formation of two mole Y_2O_3 releases 776.95 kJ/mol energy versus decomposition of 3 mol ZrO_2) according to reaction (1):

$$3ZrO_2 + 4Y \rightarrow 3Zr + 2Y_2O_3 \quad (1)$$

The difference between the two oxidation free energies can be used to compare the corresponding diffusion coefficients. According to the Arrhenius equation (Eq. 2), D_{OY} (diffusion coefficient of oxygen in yttrium) and DO_{Zr} (diffusion coefficient of oxygen in zirconium) (Eq. 3) are:

$$D_{OY}(cm^2/s) = 2\times10^{-1}\times\exp(-0.91\ eV/kBT)[35] \quad (2)$$

$$D_{OZr}(cm^2/s) = 6.61\times10^{-2}\times\exp(-184200/RT)[36] \quad (3)$$

Where T is considered 633K and kB is the Boltzmann constant, by replacing numerical values in Eq. 2, D_{OY} will be $2\times10^{-1}\times\exp(-10560/633)$ cm^2/s and D_{OZr} will be $6.61\times10^{-2}\times\exp(-22155/633)$ cm^2/s. Thus, D_{OY}/D_{OZr} will be 2.7×10^8 at 633K. This result shows that oxygen can diffuse about 0.3 million times faster in the yttrium than in the zirconium, which somehow reveals the catalytic effect of yttrium.

Besides, the diffusion coefficient of hydrogen in Y and Zr around activation temperatures (673-970 K) are 1.03×10^{-1} and 4×10^{-2} cm^2/s [37], respectively, which shows that hydrogen can diffuse 2.575 times faster.

4. Conclusion

According to the results of the tests, outcomes are as follows:

1. The final vacuum level of Y28030, Y28080, and Y36030 were 9.9×10^{-6}, 6.2×10^{-6}, and 5.98×10^{-6} mmHg, respectively, which shows the importance of the activation temperature.
2. Vacuum preserving time from 0.001 to 0.2 mmHg for Y36030, Y28030, and the no-getter was 3088, 510, and 345 seconds, respectively.
3. According to the EDS results, the amount of Zr and Co was 53.25 %Wt. and 17.58 %Wt., which were very close to the Zr_3Co phase.
4. According to the SAED pattern, some bright points represent the presence of the crystalline phases for Y36030, unlike Y28030.
5. According to the line and map scan for Y36030, in comparison with Y28030, less oxygen content was detected, which showed a higher amount of oxygen diffused into the bulk.
6. The amount of sorbed hydrogen in Y36030 and Y28030 were 1.5 and 1.05 %Wt., respectively. Remaining hydrogen was 0.71 and was 0.55 %Wt in Y36030 and Y28030, respectively.
7. The specific surface area of Y36030 and Y28030 were 75.23 and 61.27 m^2/gr, respectively. This can be

related to the nucleation and growth of nanoparticles from the amorphous phase.

Acknowledgments

This research has done in EnerMat Lab, at IROST. The authors would like to express their gratitude to their financial support.

References

[1] Xu Y., Cui J., Cui H., Zhou H., Yang Zh., Jun Du, “ZrCoCe getter film solution under controlled atmosphere for MEMS packaging”, International Conference on Advances in Energy, (AEECE-2015) China, 2015.

[2] SAES Getter, Technical Report, "St 707 Non-Evaporable Getters Activatable at Low Temperatures". https://psec.uchicago.edu/getters/St%20707%20.

[3] Benvenuti C., Chiggiato P., "Obtention of pressures in the 10−14 Torr range by means of a Zr-V-Fe non evaporable getter". Vacuum, 1993. 44: 511.

[4] Benvenuti C., Chiggiato P., "Pumping Characteristics of the St707 Nonevaporable Getter (Zr 70 V 24.6-Fe 5.4 wt %)". J. of Vacuum Science & Technology, 1996. 14: 3278.

[5] Riabova A.B., Yartys V. A., Fjellvag H., Haubackb B.C., Sørbyb M.H., "Neutron diffraction studies of Zr-containing intermetallic hydrides with ordered hydrogen sublattice.: V. Orthorhombic $Zr_3Co_{6.9}D$ with filled Re3B-type structure", J. of Alloys and Compounds, 2000. 296: 312.

[6] Heidary Moghadam A., Dashtizad V., Kaflou A., Yoozbashizadeh H., "Effect of rare earth elements on sorption characteristics of nanostructured Zr-Co sintered porous getters", J. of Vacuum, 2015, 111: 9.

[7] Zhang H., Su R., Chen D., Shi L., "Thermal desorption behaviors of helium in Zr-Co films prepared by sputtering deposition method", J. of Vacuum, 2016, 130: 174.

[8] Konishi S., Nagasaki T., Yokogawa N., Naruse Y., "Development of zirconium–cobalt beds for recovery, storage and supply of tritium", J. of Fusion Engineering and Design, 1989, 10: 355.

[9] Penzhorn R.D., Devillers M., Sirch M., "Evaluation of ZrCo and other getters for Tritium handling and storage". J. of Nuclear Materials, 1990, 170: 217.

[10] Zavaliy I.Yu., Denys R.V., erný R. Cˇ, Koval’chuck I.V., Wiesinger G., Hilscher G., "Hydrogen-induced changes in crystal structure and magnetic properties of the Zr_3MO_x (M = Fe, Co) phases". J. of Alloys and Compounds, 2005, 386: 26.

[11] Xu Y., Cui J., Cui H., Zhou H., Yang Zh., Du J., "Influence of deposition pressure, substrate temperature and substrate outgassing on sorption properties of Zr-Co-Ce getter films". J. of Alloys and Compounds, 2016, 661: 396.

[12] Bu J.G., Mao C.H., Zhang Y., Wei X.Y., Du J., "Preparation and sorption characteristics of Zr–Co–RE getter films". J. of Alloys and Compounds, 2012, 529: 69.

[13] Valdre`G., Zacchini D., Berti R., Costa A., Alessandrini A., Zucchetti P., Valdre U., "Nitrogen sorption tests, SEM-windowless EDS and XRD analysis of mechanically alloyed nanocrystalline getter materials", J. of Nanostructured Materials, 1999, 11(6): p: 821.

[14] Neelima B., Rama Rao N.V., Rangadhara V., Pandian S., "Influence of mechanical milling on structure, particle size, morphology and magnetic properties of rare earth free permanent magnetic Zr_2Co_{11} alloy". J. of Alloys and Compounds, 2016, 661:72.

[15] Sakintuna B., Lamari-Darkrim F., Hirscher M., "Metal hydride materials for solid hydrogen storage: A review", International J. of Hydrogen Energy, 2007, 32: 1121.

[16] Gregg S.J., Sing K.S.W., "Adsorption, surface area and porosity". London: Academic Press; 1982.

[17] Fattahzade. M, Kaflou. A, Dashtizad V., "Study the Effect of Praseodymium and Neodymium on Adsorption Properties for Active Gases in Non-Evaporable Zr-Co Base Chemical Getter and Comparing with Yttrium", J. of Advanced Materials and Technologies, 2018, 7: 55.

[18] Huaqin Kou W.L., Huang Zh., Sang G., Hu Ch., Chen Ch., Zhang G., Luo D., Liu M., Zheng Sh., "Effects of temperature and hydrogen pressure on the activation behavior of ZrCo", International J. of Hydrogen Energy, 2016. 41: 10811.

[19] Matolin V., Drbohlav J., Masek K. , "Mechanism of non-evaporable getter activation, XPS and static SIMS study of Zr44V56 alloy", J. of Vacuum, 2003, 71: 317.

[20] Batra I.S., Singh R.N., Sengupta P., Maji B.C., Madangopal K., Manikrishna K.V., Tewari R., Dey G.K., "Mitigation of hydride embrittlement of zirconium by yttrium". J. of Nuclear Materials, 2009, 389: 500.

[21] Heidary Moghadam A., Dashtizad V., Kaflou A., Yoozbashizadeh H., Ashiri R., Development of a nanostructured Zr_3Co intermetallic getter powder with enhanced pumping characteristics, J. of Intermetallics. 2015, 57: 51.

[22] Petti, D., Cantoni. M., Leone M., Bertacco R., Rizzi E., Activation of Zr–Co–rare earth getter films: An XPS study, Applied Surface Science, 2010, 256: 6291.

[23] Dwight A.E., Klippert T.E., Variants of Zr_3Co and their superconducting critical temperatures. Materials Research Bulletin, 1978. 13: 595.

[24] Bereznitsky M., Jacob I., Bloch J., Mintz M. H., Thermodynamic and structural aspects of hydrogen absorption in the Zr(AlxFe1−x)2 system. J. of Alloys and Compounds, 2003, 351: 180.

[25] Fisher.P.W., Tanase M., Diffusivities of hydrogen in yttrium and yttrium alloys. J. of Nuclear Materials, 1984, 122 : 1536.

[26] Hara M., Okabe T., Mori K., Watanabe K., Kinetics and mechanism of hydrogen-induced disproportionation of ZrCo. Fusion Engineering and Design, 2000, 49-50: p: 831.

[27] Szpunar J. A., Qin W., Li H., Kiran Kumar N.A.P., Roles of texture in controlling oxidation, hydrogen ingress and hydride formation in Zr alloys, J. of Nuclear Materials, 2012, 427:343.

[28] Buschow K.H.J., Bouten P.C.P., Miedema A.R., Hydrides formed from intermetallic compounds of two transition metals: a special class of ternary alloys, J. of Physics. 1982, 45:937.

[29] Sandrock G., A panoramic overview of hydrogen storage alloys from a gas reaction point of view, J. of Alloy and Compounds, 1999, 293:877.

[30] Zhang T., Zhang Y., Zhang M., Hu R., Kou H., Li J., Xue X., Hydrogen absorption behavior of Zr-based getter materials with Pd-Ag coating against gaseous impurities. International J. of Hydrogen Energy, 2016, 41: 14778.

[31] Asse-Coutrin N., Altenor S., Cossement D., Jean-Marius C., Gaspard S., Comparison of parameters calculated from the BET and Freundlich isotherms obtained by nitrogen adsorption on activated carbons: a new method for calculating the specific surface area. Microporous and Mesoporous Materials, 2008. 111: 517.

[32] Altin O., Özbelge HÖ., Dogu T., Effect of pH in an aqueous medium on the surface area, pore size distribution, density, and porosity of montmorillonite, J. of Colloid and Interface Science 1999, 217:19.

[33] Simon C. A., Scandium, Yttrium & the Lanthanides: Inorganic & Coordination Chemistry, https://doi.org/10.1002/9781119951438.eibc0195.

[34] Tejland P., Andren H.O., Origin and effect of lateral

cracks in oxide scales formed on zirconium alloys. J. of Nuclear Materials, 2012, 430: 64.

[35] Martin M., Gommel C., Borkhart C., Fromm E., Absorption and desorption kinetics of hydrogen storage alloys. J. of Alloys and Compounds, 1996, 238: 193.

[36] Benvenuti C., Chiggiato P., Pinto P.C., Vacuum properties of TiZrV non-evaporable getter films, Vacuum, 2001, 60: 57.

[37] Bakker H., Bonzel H.P., Bruff C.M., Dayananda M.A., Gust W., Horvath J., Kaur I., Kidson G.V., LeClaire A.D., Mehrer H., Murch G.E., Neumann G., Stolica N., Stolwijk, Diffusion in solid metals and alloys. Condensed Matter, 1990, 26.